

## Temperature trends at the surface and in the troposphere

Konstantin Y. Vinnikov,<sup>1</sup> Norman C. Grody,<sup>2</sup> Alan Robock,<sup>3</sup> Ronald J. Stouffer,<sup>4</sup> Philip D. Jones,<sup>5</sup> and Mitchell D. Goldberg<sup>2</sup>

Received 20 June 2005; revised 12 October 2005; accepted 7 November 2005; published 11 February 2006.

[1] This paper incorporates the latest improvements in intersatellite calibration, along with a new statistical technique, to determine the diurnal and seasonal cycles and climatic trends of 1978–2004 tropospheric temperature using Microwave Sounding Unit measurements. We also compare the latitudinal distribution of temperature trends from the surface and troposphere with each other and with model simulations for the past 26 years. The observations at the surface and in the troposphere are consistent with climate model simulations. At middle and high latitudes in the Northern Hemisphere, the zonally averaged temperature at the surface increased faster than in the troposphere while at low latitudes of both hemispheres the temperature increased more slowly at the surface than in the troposphere. The resulting global averaged tropospheric trend is +0.20 K/10 yr, with a standard error of 0.05 K/10 yr, which compares very well with the trend obtained from surface reports.

**Citation:** Vinnikov, K. Y., N. C. Grody, A. Robock, R. J. Stouffer, P. D. Jones, and M. D. Goldberg (2006), Temperature trends at the surface and in the troposphere, *J. Geophys. Res.*, *111*, D03106, doi:10.1029/2005JD006392.

### 1. Introduction

[2] The global temperature trend is difficult to measure since natural climate variability and observation errors can have random trend-like warming and cooling for limited time intervals, which can lead to errors and even mask the climatic trends. To reduce these errors and improve the accuracy of the trend, one needs to improve the data accuracy and increase the record length. Century-long surface air temperature records were used to detect a global climate trend prior to the existence of satellite measurements. More recently, the overlapping time series of satellite measurements from the Microwave Sounding Unit (MSU) have been used to detect the tropospheric temperature trend over the past 25 years [Mears *et al.*, 2003; Vinnikov and Grody, 2003; Christy and Norris, 2004]. This study uses a more accurate intersatellite calibration technique [Grody *et al.*, 2004] together with diurnal cycle corrections [Vinnikov and Grody, 2003; Vinnikov *et al.*, 2004] to improve the trend analysis. In addition to obtaining the global trend, we compare the MSU latitudinal distribution of trend with those determined from surface air temperature measurements and climate model simulations.

[3] Microwave radiometers such as the MSU measure the temperature emanating from different layers of the Earth's atmosphere by detecting the thermally emitted radiation at different frequencies within the 50- to 60-GHz portion of the oxygen band. Calibration of the radiometers is obtained by viewing cold space and an onboard warm target of known temperature at the beginning and end of every scan cycle. Between calibration periods, the MSU views the Earth and measures the upwelling thermal radiation, or brightness temperature, at four frequencies within the oxygen band. The nadir viewing measurements at 53.74 GHz (denoted channel 2) mainly respond to temperature variations in the middle troposphere, so this channel is used to monitor changes in tropospheric temperature. Besides responding best to tropospheric temperature, the near nadir measurements eliminate the need for angular (i.e., local zenith angle) adjustments of the measurements as the MSU scans from nadir, or as the satellite height changes due to orbital decay.

[4] In addition to the tropospheric contribution, approximately 10% of the radiation measured by MSU channel 2 results from changes in surface temperature and another 10% from the atmosphere above 180 hPa. It is important to recognize, however, that unlike the changes in temperature, surface emissivity only results in a 1% variation because of the compensating surface emitted and downwelling reflected radiation [Grody *et al.*, 2004]. Therefore the change in the globally averaged measurements due to temporal variations in emissivity (e.g., due to changes in sea ice, snow cover, or soil wetness) is negligibly small. Of greater importance is the diurnal variation in surface temperature due to orbital drift and the different satellite observing times. Such diurnal variations must be accounted for when constructing a time series using the 26 years of satellite measurements.

<sup>1</sup>Department of Atmospheric and Oceanic Science, University of Maryland, College Park, Maryland, USA.

<sup>2</sup>Center for Satellite Applications and Research, NOAA/NESDIS, Camp Springs, Maryland, USA.

<sup>3</sup>Department of Environmental Sciences, Rutgers University, New Brunswick, New Jersey, USA.

<sup>4</sup>Geophysical Fluid Dynamics Laboratory, NOAA, Princeton, New Jersey, USA.

<sup>5</sup>Climate Research Unit, University of East Anglia, Norwich, UK.

[5] We also recognize that the MSU channel 2 brightness temperature trend may be underestimated compared to in situ tropospheric temperature warming because of stratospheric cooling [Fu *et al.*, 2004; Fu and Johanson, 2005]. It is important to note, however, that the climate model simulations of MSU channel 2 used here include both the surface and stratospheric contributions, so that our comparisons between modeled and observed channel 2 brightness temperatures are completely valid. Stated differently, rather than adjust the channel 2 measurements we have chosen to include the surface and stratospheric contributions in the MSU climate model simulations, which are then compared directly with the satellite measurements.

[6] We take advantage of the latest improvement of intersatellite calibration [Grody *et al.*, 2004], which we apply to the MSU channel 2 measurements to enable a more accurate global temperature trend, in addition to its latitudinal distribution, over the period 1978–2004. Until now, empirical procedures have been used to intercalibrate the MSU observations. Previous researchers [Christy *et al.*, 2000; Mears *et al.*, 2003] assumed that the error in the MSU brightness temperature measurements,  $\Delta T_b$ , is directly proportional to variations of the warm target temperature used for calibration,  $T_w$ , plus a constant offset,  $\alpha$ , i.e.,  $\Delta T_b = \alpha + \beta T_w$ . However, we have shown that this empirical adjustment model which was to account for errors in the pre-launch nonlinearity coefficients does not follow from the theory and design of the MSU instruments [Grody *et al.*, 2004]. Furthermore, if statistical regression is used to estimate the correction coefficients  $\alpha$  and  $\beta$  from the observed time series of  $T_b$  and  $T_w$  [Mears *et al.*, 2003; Christy and Norris, 2004], a trend-like variation in target temperature,  $T_w$ , due to drifts in the satellite orbit can artificially modify the climatic trend in the brightness temperature  $T_b$ . Our approach to account for instrumental errors is quite different [Grody *et al.*, 2004].

## 2. Intersatellite Calibration of MSU

[7] Our analysis incorporates the MSU channel 2 brightness temperature measurements observed at nadir from the TIROS-N, NOAA-6, 7, 8, 9, 10, 11, 12, and 14 satellites, for the time interval between November 1978 and December 2004. The data were preliminary averaged over  $2.5^\circ \times 2.5^\circ$  latitude-longitude grids and over 5-day intervals (pentads) separately for ascending and descending orbits. Compared to our earlier study [Vinnikov and Grody, 2003] which only considered global averages, we do not combine MSU with AMSU (Advanced Microwave Sounding Unit: the next generation of microwave sounders) observations here, since MSU has different frequencies and, hence, different weighting functions than AMSU for the midtropospheric channels. Therefore, although the difference between AMSU and MSU brightness temperatures can be assumed to be approximately constant for global averages, this simplification cannot be applied for regional and zonal averages since then the differences depend much more on the vertical profile of air temperature, which can affect the regional and seasonal trend estimates. Also, MSU observations poleward of  $82.5^\circ\text{N}$  and  $82.5^\circ\text{S}$  have been excluded to eliminate differences in nadir viewing coverage for the a.m. and p.m. NOAA satellites, since this can result in a global

mean difference of 0.1 K between the two types of satellite observations, and subsequently lead to errors in the intersatellite calibration.

[8] To more accurately account for instrumental errors, a physically based procedure was developed by Grody *et al.* [2004] to calibrate multisatellite observations for climatic studies. If  $T_b$  is the Earth-viewing measurement, the corrected brightness temperature measurement  $T'_b$  is given by

$$T'_b = T_b - [\delta T - Z\delta U], \quad (1)$$

where the bracketed term is the calibration bias. The bias contains an offset,  $\delta T$ , that depends on the cold space and warm target calibration errors, and a parameter  $\delta U$ , which is proportional to the calibration target errors as well as the uncertainties in the instruments' nonlinearity. The  $\delta U$  parameter in equation (1) is multiplied by a  $Z$  factor,

$$Z = (T_b - T_C)(T_w - T_b), \quad (2)$$

which is a function of the measurements of Earth, cold space temperature  $T_C$ , and the warm target,  $T_w$ . Therefore, unlike the offset, the second bias adjustment  $Z\delta U$  varies in space and time as the satellite orbits the Earth. These temporal variations can have the same periodicities as the seasonal and diurnal variations of brightness temperature so that we were unable to simultaneously determine the instrumental adjustments and climatic variations using the self-consistent approach developed earlier by Vinnikov and Grody [2003], which was only used to determine the offset in the bias, i.e.,  $\delta T$ . This study uses the more accurate intersatellite calibration technique based on (1) to improve the trend analysis.

[9] The nonlinear factor  $Z(T_w, T_b)$  in (1) depends on the brightness temperature measurements, which vary with latitude, as well as on the warm target temperature. As such our technique does not need to use the temporal information associated with  $T_w$  to derive the calibration adjustment parameters, but only needs to use the latitudinal variation from two widely spaced zones to derive the bias parameters in (1). As discussed by Grody *et al.* [2004], this minimizes the possibility of including trend-like variations in  $T_w$  when deriving the calibration adjustments. Stated differently, in our approach, a nonclimatic trend in  $T_w$  cannot cause noticeable error in the calibration parameters.

[10] As discussed in detail by Grody *et al.* [2004], both  $\delta T$  and  $\delta U$  are derived using statistical analysis whereby the differences between overlapping satellite measurements are minimized with the  $Z$ -factors being the predictands. The overlapping pentads of satellite measurements can be used to obtain a multitude of equations for determining the calibration parameters. However, one must account for the fact that these individual measurements are not statistically independent. Also, as mentioned above, this procedure can introduce a nonclimatic trend in  $T_w$ . In our approach, the measurements are grouped [Wald, 1940] into two broad equal-area latitudinal bands, joined at a common latitude, and temporally averaged over an extended time period comprising many pentads. The long-time average reduces the effect of any trends in the warm target temperature on the analysis as well as the noise

**Table 1.** Offsets ( $\delta T$ ) and Parameters ( $\delta U$ ) in Equation (1) Used to Adjust Pentad and  $2.5^\circ \times 2.5^\circ$ -Averaged Observed MSU Channel 2 Brightness Temperatures for Ascending and Descending Orbits<sup>a</sup>

Parameter	$\delta T$ , K	$\sigma_{\delta T}$ , K	$\delta U$ , $10^4 \text{ K}^{-1}$	$\sigma_{\delta U}$ , $10^4 \text{ K}^{-1}$
TIROS-N	0.42	0.05	-0.20	0.07
NOAA-6	0.06	0.04	-0.48	0.05
NOAA-7	0.36	0.04	-0.33	0.05
NOAA-8	-0.12	0.04	-0.86	0.06
NOAA-9	-0.14	0.03	-1.08	0.05
NOAA-10	0	0	-0.85	0.06
NOAA-11	-0.17	0.03	-0.73	0.06
NOAA-12	0.29	0.03	-0.50	0.07
NOAA-14	0.33	0.03	-0.55	0.07

<sup>a</sup>Here  $\sigma_{\delta T}$  and  $\sigma_{\delta U}$  are standard errors of these parameters.

introduced by the nadir measurements viewing the same location at different times.

[11] In addition to calibration errors, some of the difference between satellite measurements is due to diurnal variations. To reduce the effect of diurnal variations on the measurements, the ascending and descending orbital brightness temperatures are averaged together. This filters all odd harmonics in a Fourier series representation of the diurnal variation, leaving the second harmonic as the dominant term. The bias parameters are obtained by applying (1) to each of the two latitudinal zones and each of the 12 overlapping satellite intervals, assuming that the corrected brightness temperatures are approximately equal for each pair of overlapping satellites, and minimizing the difference between overlapping measurements. Although we do not know a priori the calibration accuracy of any instrument we chose to reference all offsets to the MSU on NOAA-10 (i.e.,  $\delta T_{NOAA-10} \equiv 0$ ), since the referenced offset adds the same constant to all MSU measurements, thereby not affecting the use of the data for climatic trend analysis. However, a change in the  $\delta U$  parameter for one MSU changes the bias parameters for all other instruments nonuniformly. Therefore an incorrect reference for  $\delta U$  can significantly alter the trend of the MSU time series so that the best estimates of this parameter were obtained for each instrument using the least squares technique described by Grody *et al.* [2004]. The calibration parameters estimated by Grody *et al.* [2004] have been recomputed here by excluding all observations for latitudes higher than  $82.5^\circ\text{S}$  and  $\text{N}$ ; the new parameters are given in Table 1. The changes in the parameters are noticeable, but they do not result in significant change in the trend estimates. Also, the standard errors of the estimates are small compared to real uncertainties in their values.

[12] As discussed by Grody *et al.* [2004], the averaged measurements for two wide latitudinal belts have been used for intersatellite calibration of MSU radiometers since they provide the maximum difference in brightness temperatures. These two zones were also chosen since they have equal areas and together fully cover the globe. The seasonal-diurnal patterns of the expected value for these two zones are discussed in the next sections.

### 3. Methodology of Trend Analysis

[13] The model used here to analyze the time series contains a linear climatic trend in addition to seasonal and

diurnal cycles, and has been described earlier by Vinnikov and Grody [2003] and Vinnikov *et al.* [2004]. In summary, we express the observed measurements  $y(t)$  at time  $t$  as the sum of two components,

$$y(t) = Y(t) + y'(t), \quad (3)$$

where the expected value  $Y(t)$  contains the seasonal and diurnal variations as well as the climatic trend, while its residual (or anomaly, in the language of climatologists)  $y'(t)$  is mostly related to natural climate variability, and contains nonperiodic atmospheric variations such as those due to volcanic eruptions and El Niño and La Niña events. The expected value of the observed variable is

$$Y(t) = A(t) + tB(t), \quad (4)$$

where  $A(t)$  and  $B(t)$  are periodic functions which are approximated as the product of two finite Fourier series, one having seasonal harmonics while the other has diurnal harmonics,

$$A(t) = \left[ \sum_{k=0}^K (a_k \sin \Omega_k t + b_k \cos \Omega_k t) \right] \cdot \left[ \sum_{n=0}^N (a'_n \sin \psi_n t + b'_n \cos \psi_n t) \right] \quad (5a)$$

$$B(t) = \left[ \sum_{l=0}^L (c_l \sin \Omega_l t + d_l \cos \Omega_l t) \right] \cdot \left[ \sum_{m=0}^M (d'_m \sin \psi_m t + d''_m \cos \psi_m t) \right]. \quad (5b)$$

[14] The left-most bracketed term in  $A(t)$  characterizes the diurnal variation of surface temperature, so that it contains harmonics at frequencies  $\Omega_k = 2\pi k/H$  whose fundamental period  $H = 1$  day. This diurnal variation is modulated by the second bracketed term, which characterizes the seasonal variation of temperature and contains harmonics at frequencies  $\psi_n = 2\pi n/T$  whose fundamental period  $T = 1$  year. Mechanisms such as vertical convection couple the surface temperature with the lower atmosphere so that  $A(t)$  also represents the midtropospheric temperature observed by microwave temperature sounders. Less obvious is the physical basis of the second term in (4) which contains a linear trend that is varied by  $B(t)$  to account for possible seasonal and diurnal variations. The upper limits  $N$  and  $M$  are the number of harmonics needed to approximate the seasonal variations, while  $K$  and  $L$  are the number of harmonics needed to approximate the diurnal variations in  $A(t)$  and  $B(t)$ .

[15] The product of the two Fourier series in (5a) and (5b) can also be written as a single series containing harmonics at frequencies  $\Omega_n$  and  $\psi_n$  as well as their sum and differences, while the coefficients are products of  $a_k$  and  $a'_n$  for example,

$$A(t) = \sum_{i=0}^{I_X} [\hat{a}_i \sin \omega_i t + \hat{b}_i \cos \omega_i t] \quad (6a)$$

$$B(t) = \sum_{j=0}^{J_X} [\hat{c}_j \sin \omega_j t + \hat{d}_j \cos \omega_j t], \quad (6b)$$

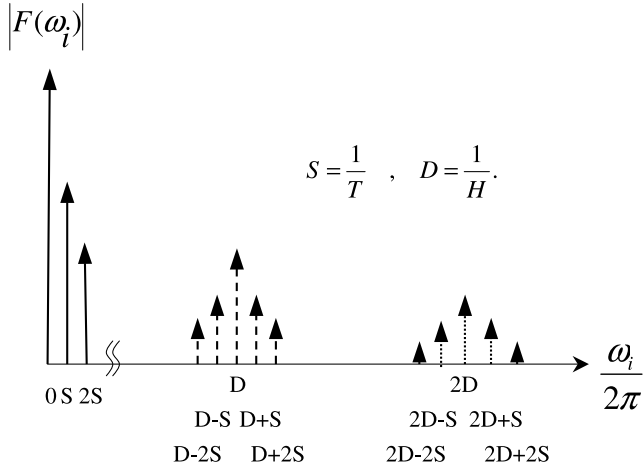


**Figure 1.** Schematic illustration of amplitude spectrum,  $|F(\omega_i)|^2 = a_i^2 + b_i^2$ , showing all of the components up to the second harmonic in the seasonal and diurnal cycles.

where  $\omega_0 = 0$ ,  $\omega_1 = \psi_1$ ,  $\omega_2 = \Omega_1$ ,  $\omega_3 = 2\psi_1$ ,  $\omega_4 = 2\Omega_1$ , etc. As shown in Figure 1, a total of 24 frequency components (sines and cosines) exist up to the second harmonic, of which four contain the first harmonic of the diurnal and seasonal cycles, while the other 20 terms involve sum and difference frequencies. Therefore, unlike the two individual Fourier series in (5a) and (5b), the frequencies of the combined series are no longer equally spaced due to mixing of the annual and diurnal periods. As such, the new coefficients in (6a) and (6b) are no longer independent of one another as in a Fourier series representation. Second, (4) contains a linear trend, so that the combined waveform,  $A(t) + t B(t)$ , is no longer periodic with annual periodicity  $T$  and the different harmonic components in  $A(t)$  and  $B(t)$  are also coupled together. Third, the observations occur at different times of the day as the satellite drifts. For all of these reasons the coefficients must be obtained numerically and are interdependent.

[16] For analysis of the temperature time series (4), it is generally only necessary to consider frequency components up to the second harmonic in the seasonal and diurnal cycles for  $A(t)$  and only up to the first harmonic in the diurnal cycle for  $B(t)$ . Furthermore, the daily and seasonal oscillations nearly average out to zero when taking the yearly averaged expected value over the complete 26-year time series so that  $\langle Y \rangle = \hat{b}_0 + \hat{d}_0 t$ , where  $\hat{d}_0$  is the long-term climatic trend in annual averages and  $\hat{b}_0$  is the detrended value of  $\langle Y \rangle$ . However, a complete set of coefficients, up to the second harmonic, is needed to display the diurnal and seasonal variations of the expected value. Also, as mentioned previously, the expected value coefficients are dependent so that the addition of a second harmonic component in  $A(t)$  can modify the linear trend coefficient,  $\hat{d}_0$ .

[17] Because we know nothing a priori about the residual term  $y'(t)$ , the unknown coefficients  $\hat{a}_i$ ,  $\hat{b}_i$ ,  $\hat{c}_j$ ,  $\hat{d}_j$  in (6) are first estimated using the ordinary least squares technique,

$$\mathbf{X} = [\mathbf{M}'\mathbf{M}]^{-1}\mathbf{M}' \cdot \mathbf{y} \quad (7a)$$

where

$$\mathbf{X} = |\hat{a}_0 \cdots \hat{a}_{I_X} \quad \hat{b}_0 \cdots \hat{b}_{I_X} \quad \hat{c}_0 \cdots \hat{c}_{J_X} \quad \hat{d}_0 \cdots \hat{d}_{J_X}|^t, \quad (7b)$$

$$\mathbf{y} = |y(t_1)y(t_2) \cdots y(t_P)|^t, \quad (7c)$$

$$\mathbf{M} = \begin{vmatrix} c_{1,0} \cdots c_{1,I_X} & s_{1,1} \cdots s_{1,I_X} & u_{1,0} \cdots u_{1,J_X} & v_{1,1} \cdots v_{1,J_X} \\ c_{2,0} \cdots c_{2,I_X} & s_{2,1} \cdots s_{2,I_X} & u_{2,0} \cdots u_{2,J_X} & v_{2,1} \cdots v_{2,J_X} \\ \cdots & \cdots & \cdots & \cdots \\ c_{P,0} \cdots c_{P,I_X} & s_{P,1} \cdots s_{P,I_X} & u_{P,0} \cdots u_{P,J_X} & v_{P,1} \cdots v_{P,J_X} \end{vmatrix}, \quad (7d)$$

with

$$c_{i,j} = \text{Cos}(\omega_j t_i), \quad s_{i,j} = \text{Sin}(\omega_j t_i), \quad u_{i,j} = t_i c_{i,j}, \quad v_{i,j} = t_i s_{i,j}. \quad (7e)$$

where  $\mathbf{t}$  is the transpose and  $-\mathbf{1}$  denotes the inverse matrix operator. In (7a), the column matrices  $\mathbf{X}$  and  $\mathbf{y}$  contain the respective unknown coefficients and  $P$  temporal measurements, while the rectangular matrix  $\mathbf{M}$  contains the sine and cosine terms computed at the different harmonic frequencies and observation times.

[18] The ordinary least squares technique assumes independent observations with equal variances of residuals, i.e.,

$$\overline{y'(t_1)y'(t_2)} = 0 \quad \text{for } t_1 \neq t_2, \quad \text{and} \quad \overline{(y'(t))^2} = \sigma^2 = \text{const}, \quad (8)$$

where the overbar denotes an ensemble average. This simplification has been applied in our earlier analyses [Vinnikov and Grody, 2003; Vinnikov et al., 2004] and will be used initially here as well. However, as discussed in the next section, we will also use the statistical properties of the residuals  $y'(t)$  to improve the accuracy of the coefficients by applying a generalized least squares technique to account for correlations in the measurements. The generalized least squares solution for the coefficients is given by [e.g., Jenkins and Watts, 1968]

$$\mathbf{X} = [\mathbf{M}'\mathbf{V}^{-1}\mathbf{M}]^{-1}\mathbf{M}'\mathbf{V}^{-1} \cdot \mathbf{y}, \quad (9)$$

where  $\mathbf{V}$  is the covariance of the residuals, which is a symmetric square matrix,

$$\mathbf{V} = \begin{vmatrix} R(0) & R(\tau_{12}) & R(\tau_{13}) & \cdots & R(\tau_{1P}) \\ R(\tau_{21}) & R(0) & R(\tau_{23}) & \cdots & R(\tau_{2P}) \\ \vdots & \vdots & \vdots & \ddots & \vdots \\ & & & & R(0) \end{vmatrix}, \quad (10)$$

whose elements will be discussed next.

#### 4. Global and Regional Trends of MSU Measurements

[19] We calculated pentad averages of the brightness temperature measurements separately for the ascending

**Table 2.** The 1978–2004 MSU Channel 2 Brightness Temperature Trend Estimates for Eight Regions of the Globe, Using Ordinary and Generalized Least Squares<sup>a</sup>

Region	$T_{\text{mean}}$ , K	$\sigma$ K	Least Squares for Independent Data		Least Squares for Correlated Data	
			$r(\tau)\tau = 12$ hours	Trend, K/10 yr	Trend, K/10 yr	$\sigma_{\text{Trend}}$ , K/10 yr
High latitudes	244.6	0.25	0.96	0.19	0.18	0.03
Low latitudes	256.6	0.31	0.99	0.26	0.21	0.07
Global	250.7	0.22	0.98	0.22	0.20	0.05
Antarctic	224.3	1.34	0.99	−0.06	−0.06	0.09
Arctic	237.0	1.33	0.99	0.27	0.31	0.07
Tropical oceans	255.7	0.34	0.96	0.25	0.21	0.06
North Africa	258.5	0.54	0.93	0.31	0.29	0.06
Tibet	250.2	0.96	0.84	0.32	0.32	0.06

<sup>a</sup>Number of harmonics used to approximate seasonal and diurnal cycles in  $A(t)$  and  $B(t)$  are equal to  $K = N = M = 2$ ,  $L = 1$  (see equation (5)).

and descending orbits for each of the nine satellites carrying MSU instruments. The measurements have also been averaged separately for eight geographical regions: high ( $30^\circ < |\varphi| < 82.5^\circ$ ) and low latitudes ( $|\varphi| \leq 30^\circ$ ) used for calibration [Grody *et al.*, 2004]; globally ( $|\varphi| < 82.5^\circ$ ), which is close to that used by Vinnikov and Grody [2003]; three regions generally having a weak diurnal cycle, Arctic ( $75^\circ\text{N} < \varphi < 82.5^\circ\text{N}$ ), Antarctic ( $75^\circ\text{S} < \varphi < 82.5^\circ\text{S}$ ), and tropical ocean ( $15^\circ\text{S} < \varphi < 25^\circ\text{S}$ ); and two regions generally having a strong diurnal cycle, North African Saharan desert ( $10^\circ\text{W}–30^\circ\text{E}$ ,  $10^\circ\text{N}–25^\circ\text{N}$ ), and the Tibetan plateau ( $75^\circ\text{E}–110^\circ\text{E}$ ,  $25^\circ\text{N}–45^\circ\text{N}$ ). The regions with the weakest and strongest diurnal cycles were selected based on work by Dai and Trenberth [2004]. We also conditionally assumed that the time of observation is equal to the equator crossing time and does not depend on latitude. Related information for NOAA polar orbiters was obtained from Ignatov *et al.* [2004].

[20] The ordinary least squares technique for independent observations was used to compute the expected value coefficients [Vinnikov and Grody, 2003; Vinnikov *et al.*, 2004], where Table 2 lists the trend estimates for each of the eight geographical regions. In addition to the expected value, the residuals  $y'(t) = y(t) - Y(t)$  have also been computed. However, the residuals represent meteorological anomalies which we consider to be stationary so that the lag-covariance function of pentad and spatially averaged brightness temperatures depends only on the time difference  $\tau = |t_2 - t_1|$ , i.e.,

$$R(\tau) = \sigma^2 r(\tau), \quad (11)$$

where  $\sigma^2$  is the empirically estimated variance, and  $r(\tau \neq 0)$  is the empirically estimated lag correlation for different lags  $\tau$  using pentad averages of brightness temperature observed during ascending or descending parts of the satellite orbit. Such pentad-averaged data are attributed to the middle days of each pentad. Small differences in the lags, related to differences in equator crossing time of satellites, are ignored. We also consider that the temporal (pentad) and spatially (region) averaged variance is  $\sigma^2 = \sigma_o^2 + \delta^2$  where  $\sigma_o^2$  is the real variance of the residual and  $\delta^2$  is the variance of the random error of measurement. The  $\delta^2$  for each time series are estimated as  $\delta^2 = [1 - r(\tau \rightarrow 0)] \sigma^2$  where it is assumed that  $r(\tau \rightarrow 0) = r(\tau = 12\text{h})$ , estimated to be the correlation coefficient between pentad averages for ascending and descending orbits (given in Table 2). The

estimated lag-correlation functions for the eight selected regions are shown in Figure 2 and will be used in the generalized least squares solution (9) to improve the expected value coefficients. However, before being used, these empirically estimated lag-correlation functions have been multiplied by Hann's correlation window with a cut point at lag = 365 days.

[21] From November 1978 to December 2004, the climatic trends in the MSU channel 2 brightness temperature for the eight geographical regions have been estimated simultaneously with diurnal cycle corrections using a generalized least squares technique that accounts for dependent data using the lag-covariance functions of the residuals estimated above. The means, standard deviations and trend estimates are also shown in the Table 2. For the tropical half of the globe, the generalized least squares technique provides a somewhat smaller climatic trend estimate of

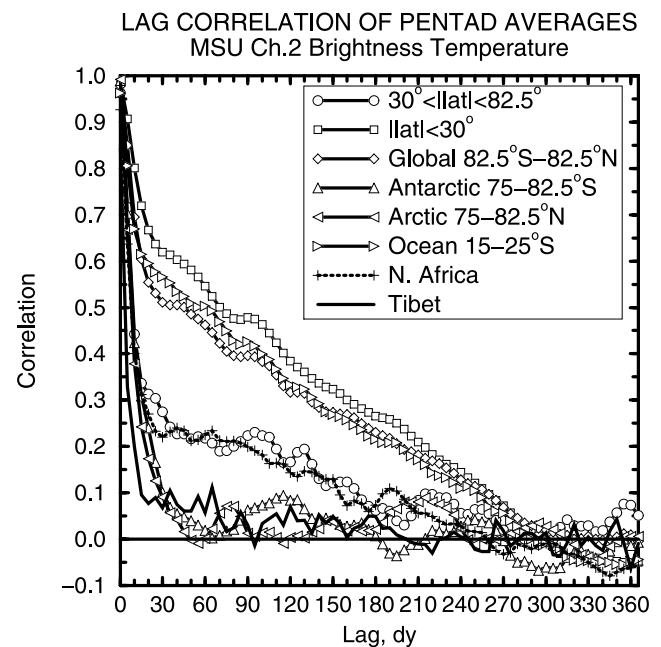


**Figure 2.** Empirically estimated lag correlations of pentad-averaged MSU channel 2 brightness temperatures for eight selected regions. These functions are used in constructing the covariance matrix (equation (10)), which is used in the generalized least squares technique (see equation (9)).

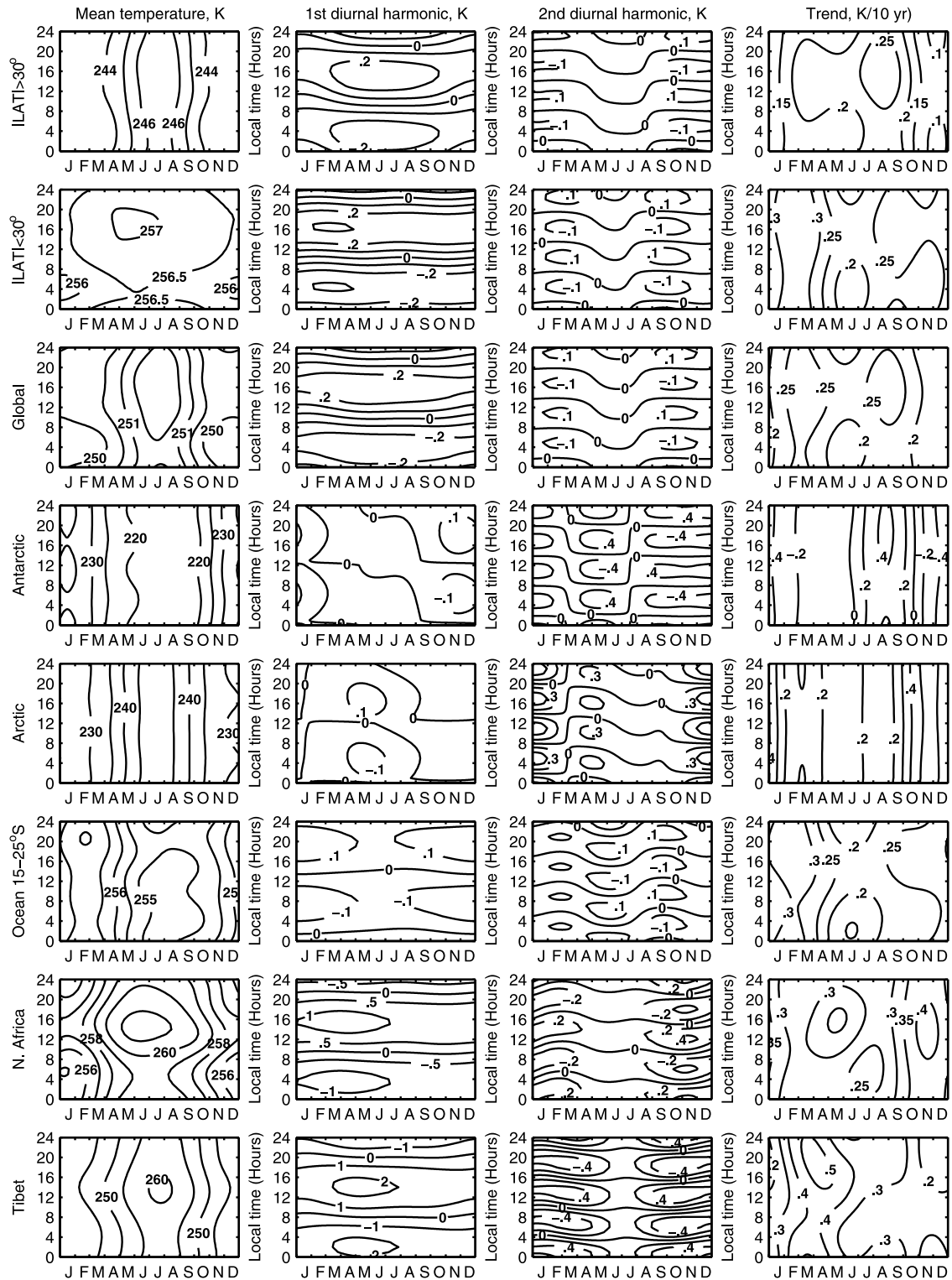


**Figure 3.** Estimates of seasonal and diurnal variations in the multiyear mean temperature, in the first and second harmonics of the diurnal cycle, and in the trend  $B(t)$ , obtained from ordinary least squares for independent observations.

+0.21 K/10 yr compared to +0.26 K/10 yr when using the ordinary least squares technique. Also, the global trend estimates decreases from +0.22 K/10 yr to +0.20 K/10 yr when accounting for dependent measurements. The differences in the trend estimates for the other regions are relatively smaller and therefore of less importance.

[22] To better illustrate the effect of taking into account the lag-correlation of the residuals, we calculated comparisons between the expected value obtained using ordinary least squares and those obtained using the generalized least squares method. Using the ordinary least squares approach, Figure 3 shows contour plots of the mean temperature

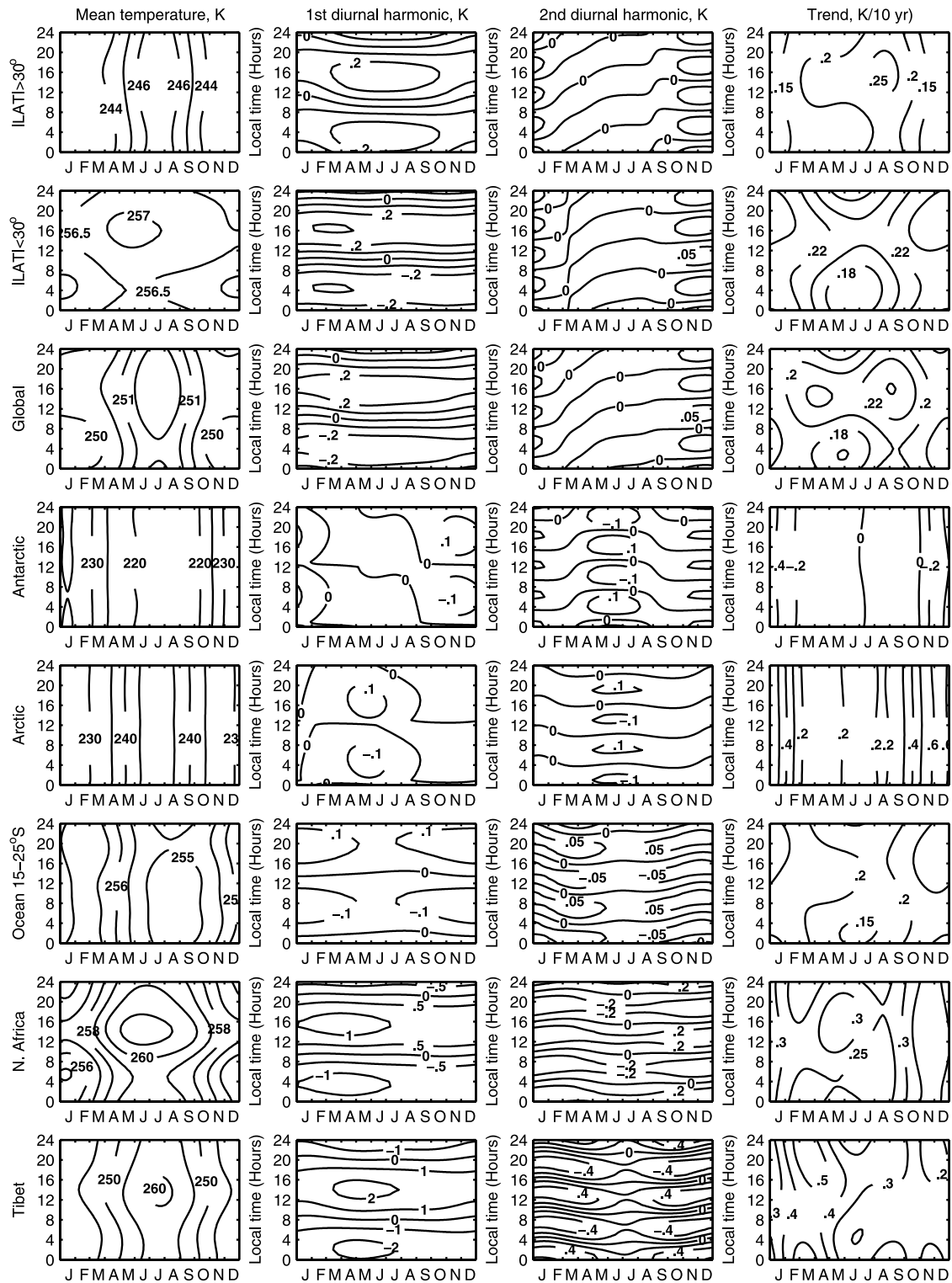


**Figure 4.** Estimates of seasonal and diurnal variations in the multiyear mean temperature, in the first and second harmonics of diurnal cycle, and in the trend  $B(t)$ , obtained from generalized least squares for correlated observations.

together with the first and second harmonics of the diurnal cycle in  $A(t)$ , and the trend,  $B(t)$ , for each of the eight regions, plotted as a function of time. Figure 4 shows the same estimates obtained using the generalized least squares technique. There are no noticeable differences (Figures 3

and 4) between estimates of the mean value and first harmonic of the diurnal cycle. However, the amplitude of the second harmonic of the diurnal cycle looks to be overestimated when the autocorrelation of the residuals is not taken into account. This is particularly noticeable in the

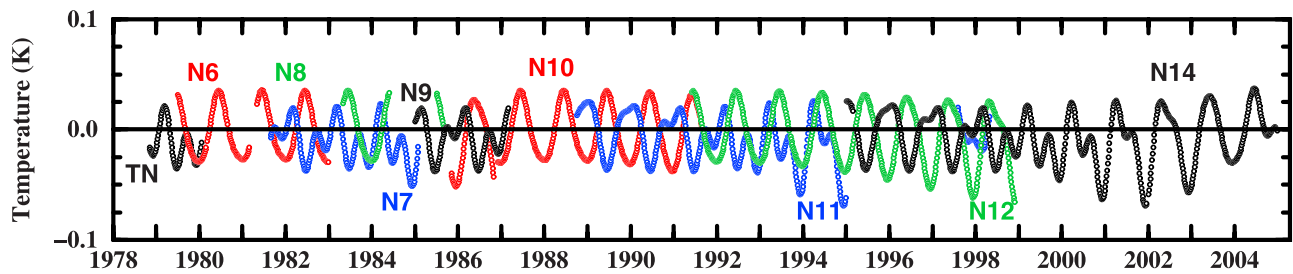


**Figure 5.** Effect of changes in equator crossing time on computed daily averages in global and pentad averaged MSU channel 2 brightness temperatures observed from NOAA satellites. This plot only contains the contributions from the second harmonic components, with the first harmonic seasonal and diurnal components removed.

tropics, which has the largest scale of temporal autocorrelation (see Figure 2) and very small diurnal cycle amplitudes. Conversely, the improvement obtained when taking into account the autocorrelation is relatively smaller for Sahara and Tibet, where these regions have the largest second harmonic for the surface air temperature. Since the coefficients are coupled, changes in the second harmonic component in  $A(t)$  produce noticeably different trend estimates when comparing the ordinary and general least squares result. It is also quite clear that by taking into account the autocorrelation in the observed data we obtain more accurate estimates of all parameters, including the amplitude of the second harmonic of the diurnal cycle and climatic trend.

[23] It is important to note that the changes in the local equator crossing time of the satellite orbits are automatically taken into account in our analysis of the expected value, since the observation times are explicitly contained in the  $\mathbf{M}$  matrix. For polar orbiters, which make observations twice a day, the changes in local equator crossing time can however affect the calculations of the second harmonic of both the diurnal cycle as well as the seasonal cycle. As an example of this effect, Figure 5 shows the time series of the globally averaged expected value of MSU channel 2 after removing the first harmonic of the diurnal and seasonal cycles, along with the trend term,  $B(t)$ , in (4). Note the strong seasonal variations from the second harmonic, which often have different signs for different satellites. It is interesting that the total effect of these variations on the global trend estimate is negligibly small, being less than 0.01 K/10 yr. Corrections of the observed data for equator crossing time are much larger however for regions with strong diurnal cycles, as in North Africa and Tibet, where amplitudes of the second harmonic of the diurnal cycle are up to four times larger than they are for global averages (see Figure 4).

[24] The statistical technique that we use here to estimate the expected value  $Y(t)$  is linear so that the spatial average of  $Y(t)$  over different geographical regions is equal to the combined spatial average over all regions. The estimates in Figures 3 and 4 were obtained for selected regions and latitude bands, where we shall now examine the zonal averages.

## 5. Time Series of Zonal Averages of MSU Channel 2 Brightness Temperature

[25] In addition to obtaining global averages, we computed zonal averages over 10-degree latitudinal bands using

the time series of pentad averages. Again, we determine the coefficients in the expected value  $Y(t)$  and residuals  $y'(t)$  using the ordinary least squares technique. The residuals are then used to estimate the lag-covariance functions for each zone, after which the generalized least squares technique is applied to obtain the final estimates of the expected value coefficients. As in the work of Vinnikov and Grody [2003], the number of harmonics for the seasonal and diurnal cycles in  $A(t)$  and  $B(t)$  are  $M = N = K = 2$ ,  $L = 1$ . For each latitude zone, Figure 6 displays the time series of the pentad averaged MSU channel 2 brightness temperature measurements, which includes the expected value and residual terms. All adjustments for calibration and time of observation have been made in these time series. Also shown is a very small sloping line which is the climatic trend in annual averages, whose slope is almost unrecognizable compared to the seasonal variations. Furthermore, the anomalies are also almost unrecognizable from these seasonal variations. Figure 7 shows the time series of the anomalies  $y'(t)$  for each latitude zone. They represent real climatic process but all that we can see in these time series are a few well-known El Niño/La Niña events in low latitudes and noise amplification toward the poles.

## 6. Latitudinal Distribution of Trends

[26] Figure 8 shows the latitudinal distribution of the trend of annual averages based on this latest calibration and analysis procedure. The observed MSU channel 2 brightness temperature trend was between +0.2 K/10 yr and +0.3 K/10 yr north of 30°S, but decreased south of this latitude until it became a small negative value. The vertical bars in the figure display the root mean square error of the trend estimate at each 10° latitude band due to climate variability. However, uncertainties in intersatellite calibration can introduce additional errors in these trend estimates.

[27] For comparison purposes, Figure 8 also displays the trends in the observed surface air temperature, based on the combined land surface air [Jones and Moberg, 2003] and marine [Rayner et al., 2003] sea surface temperature anomalies from a 1961–1990 base period. The same trend estimate for all of Antarctica south of 65°S, land only, is plotted twice at 70°S and 80°S. As for the MSU trend, the vertical bars display the root mean square error of the trend estimates for surface air temperature based on natural climate variability. These data are less accurate over data-sparse areas such as the sea-ice-covered oceans and polar

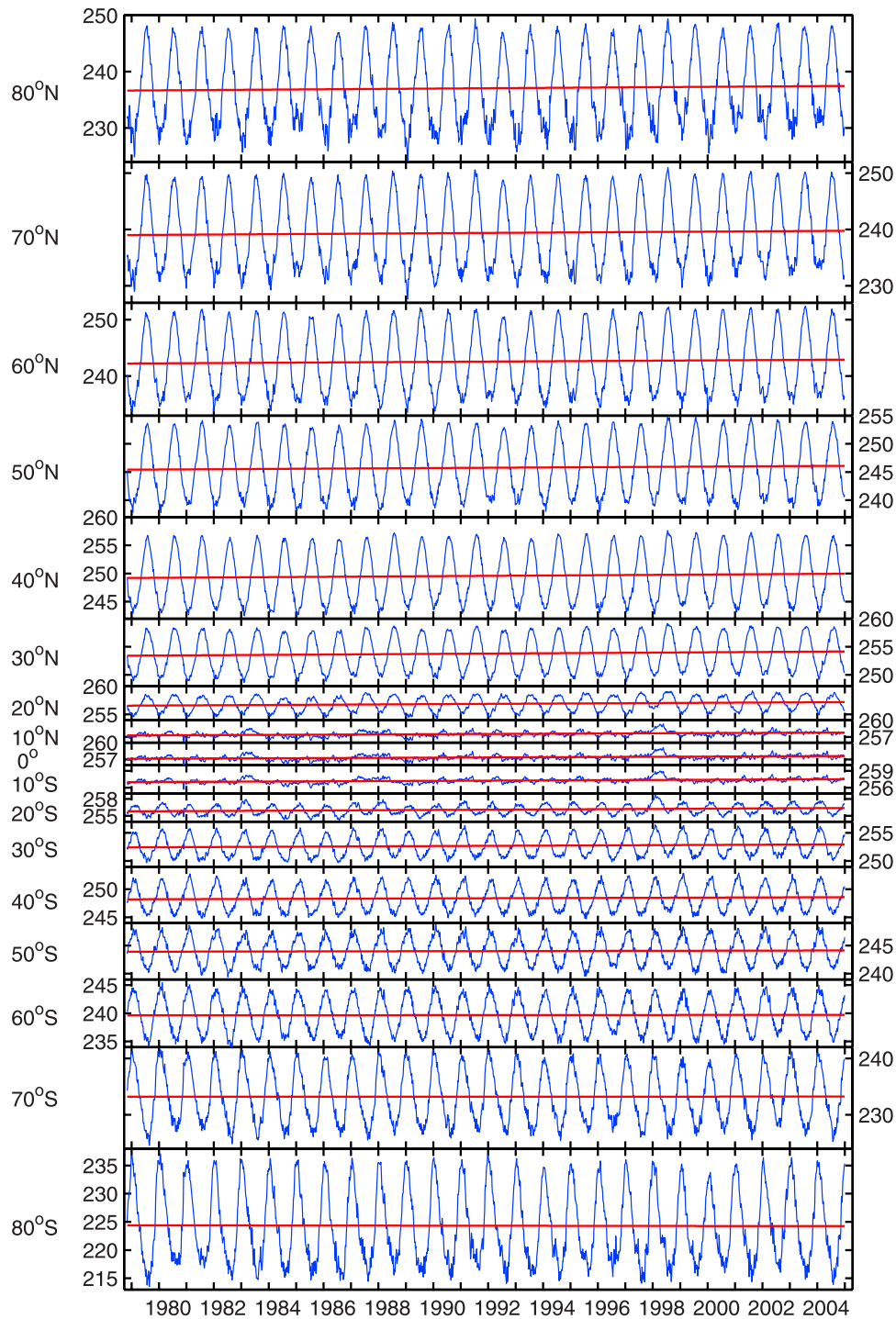


**Figure 6.** Expected value and anomalies combined of the pentad and zonally averaged MSU channel 2 brightness temperature. The nearly horizontal lines are the climatic trend in annual averages.

regions, which have few permanent land-based meteorological stations. The root mean square errors of the MSU tropospheric trends and surface trends are greater at high latitudes because of the increased local temperature variability and the decreased zonal areas, which amplify the variability of zonal averages at high latitudes [Vinnikov, 1986].

[28] The tropospheric trends obtained from the MSU and the surface air temperature trend have almost the same

global mean, but display different latitudinal patterns in Figure 8. At low latitudes, the tropospheric trend exceeds the surface air temperature trend, whereas the surface warming greatly exceeds the tropospheric warming trend north of  $25^{\circ}\text{N}$ . This latter feature is consistent with a more stable temperature structure with increasing latitude, which tends to decouple the surface layer from the troposphere, and is not significantly altered by the small warming trends. However, the trends have different directions in

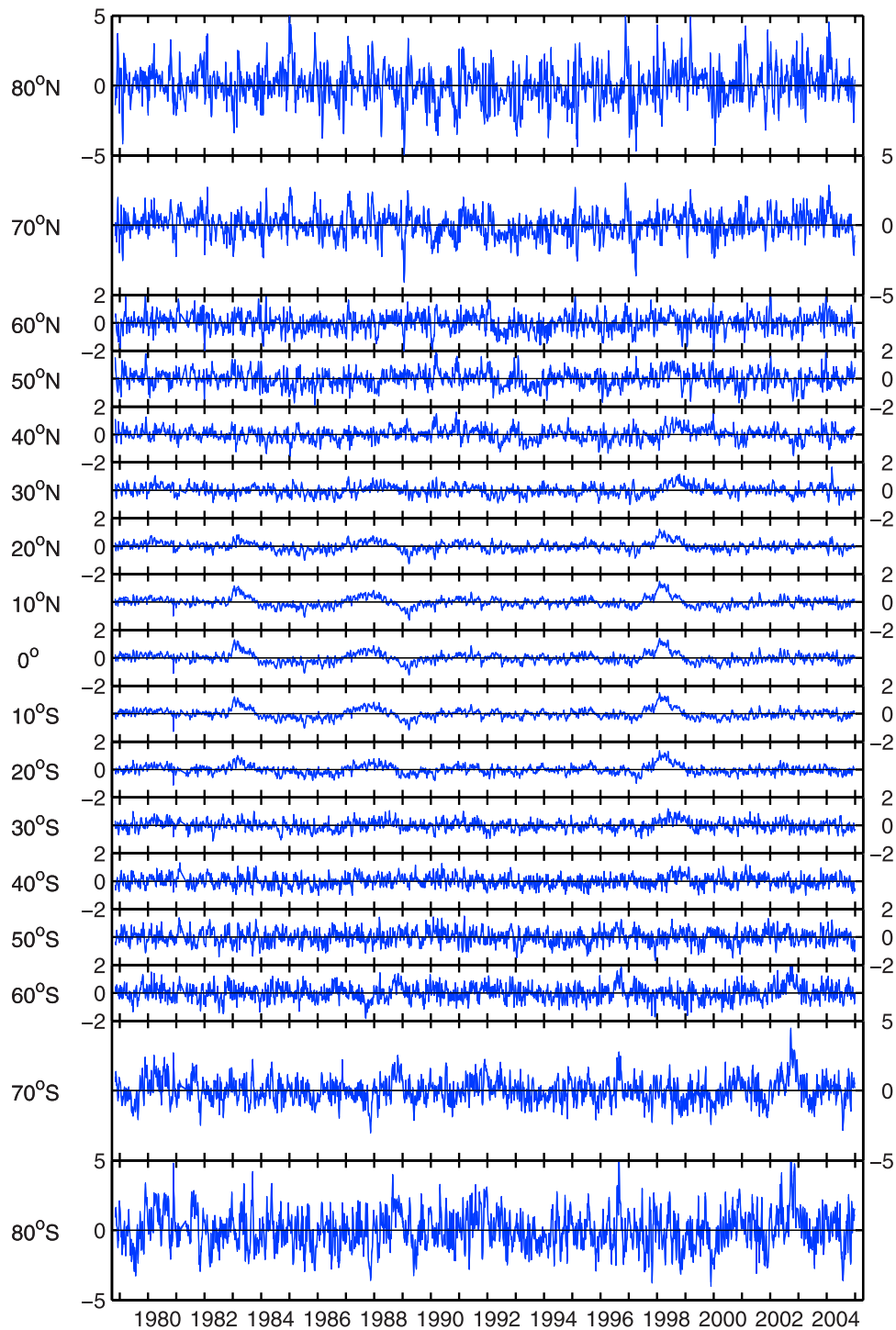


**Figure 7.** Time series of detrended pentad and zonal averaged anomalies of MSU channel 2 brightness temperature.

the Antarctic region. Owing to the high elevation ice sheets, the surface temperature contributions in the MSU channel 2 brightness temperatures are much larger than 10% so that one would expect to see similar features in both the MSU and surface data. However, in the 65°S–85°S zone the surface data over Antarctic continent are only based on a small number of the permanent stations which are less representative of the Antarctic region than the satellite observations. Of course, as was discussed

earlier, we can speculate that it is reasonable to expect larger differences between the surface record and MSU channel 2 for regions with lower tropopause heights. To further examine the physical reasons for the observed patterns, we turn to our best theoretical understanding of the climate system, which is based on an atmosphere-ocean general circulation model.

[29] Here we use the Geophysical Fluid Dynamics Laboratory (GFDL) climate model [Manabe *et al.*, 1991;

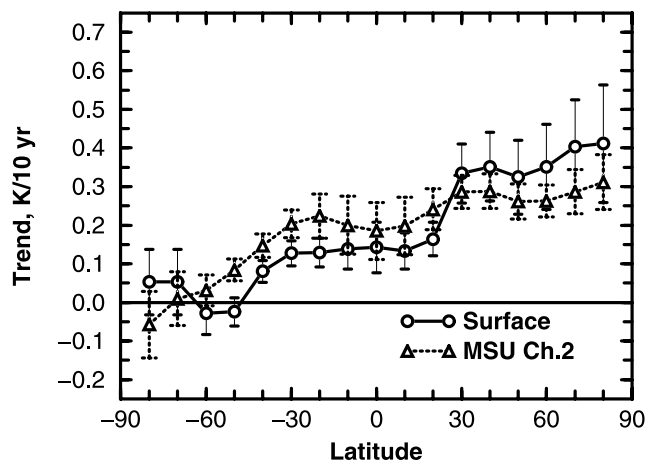


**Figure 8.** Zonally averaged 1978–2004 surface and satellite (MSU channel 2) observed air temperature trends. The vertical bars display the root mean square error of these trend estimates.

*Delworth et al.*, 2002]. We use these results as an example and expect that most climate models would produce similar trends [*Cubasch et al.*, 2001; *Santer et al.*, 2005]. Specifically, we use ensemble runs of the R30 version of this model, forced by observed changes of  $\text{CO}_2$  and sulfate aerosols [*Delworth and Knutson*, 2000; *Delworth et al.*, 2002]. Three runs of the GFDL model having different initial states, but with the same forcing, show the 1978–2004 surface warming trend to be about  $+0.2 \text{ K}/10 \text{ yr}$ , which is close to the observed surface trend of  $+0.17 \text{ K}/10 \text{ yr}$ . To simulate the corresponding MSU channel 2 trend we use the GFDL modeled atmospheric and surface temperatures, surface pressure, and sea ice thickness as input to the radiative transfer model of *Grody et al.* [2004]. The surface emissivity in this computation was assumed to be 0.95 for land and sea ice (thicker than 2 cm) and 0.53 for water surfaces. Also included is the effect of changing sea ice extent on the emissivity and resulting microwave brightness temperatures [*Swanson*, 2003]. Figure 9 shows the 1978–2004 ensemble averaged trend estimates for the GFDL modeled surface air temperature and simulated MSU channel 2 trends. Errors in these trend estimates due to the natural variability of climate change are computed using the 900-year control run of the same model.

[30] The latitudinal dependence of the modeled trends in Figure 9 and the observed trends in Figure 8 have similar features. As with the observed trends, the modeled surface temperature trend is also smaller than that of simulated MSU in the low latitudes and larger in the high latitudes of the Northern Hemisphere. The absence of thermal convection in very cold climatic conditions appears to decouple the surface temperature and free atmosphere trends. This is why we do not see polar amplification in the middle troposphere and in the MSU brightness temperatures. However, the polar amplification in the Northern Hemisphere in the modeled surface temperature is stronger than in the observed data. As a result, the modeled MSU trend does not decrease with increasing latitude. Still, the agreement between the observed and modeled MSU trend

north of  $45^\circ\text{S}$  is remarkable. There is also no cooling trend found in the modeled temperatures at high latitudes in the Southern Hemisphere. We can speculate that ozone depletion is responsible for the Antarctic cooling in the free atmosphere [e.g., *Thompson and Solomon*, 2002], which is not included in the model. In addition to not including ozone depletion, many other important radiative forcings are not included such as volcanic eruptions, indirect effect of aerosols, direct aerosol effects due to black and organic carbons, and the effects due to land surface changes and many other potential agents capable of changing climate. These factors may be responsible for the differences between the observed and modeled trends. However, the largest well understood forcings [*Ramaswamy et al.*, 2001] are included in the model integrations used here. The indirect effect has very large uncertainties [*Ramaswamy et al.*, 2001].

[31] Previous work showed larger differences between the climatic trends of temperature measured by the microwave satellite instruments and those determined from surface observations [*Wallace et al.*, 2000]. Our improvements in the intersatellite calibration of the MSU instruments have resolved much of the difference between the satellite measurements and surface observations. This consistency between observations has been further strengthened by the correlation observed with climate models. The high correlation between observations and modeled results is shown in Figure 10 by plotting the difference between the surface air temperature and MSU brightness temperature for both the observed and modeled results of Figures 8 and 9. The error bars shown for the modeled results were computed from the same 900-year control run and represents the effect of natural climate variability. Unfortunately, however, error bars cannot be estimated for the observed trends because of the very short period of observations. However, the similarity of two curves, particularly between latitudes of  $\pm 60^\circ$ , gives us confidence in both the observations and model results.

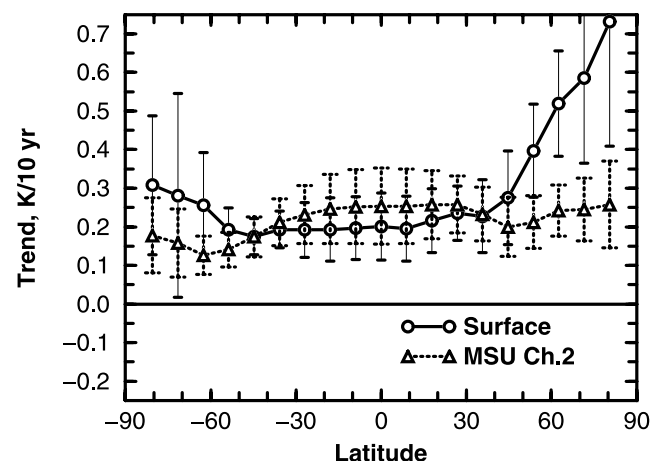


**Figure 9.** Zonally averaged 1978–2004 surface and satellite (MSU channel 2) modeled air temperature trends, from the GFDL R30 climate model ensemble run forced by changes in  $\text{CO}_2$  and sulfate aerosol [*Delworth and Knutson*, 2000; *Delworth et al.*, 2002]. The vertical bars display the root mean square errors of these trend estimates.

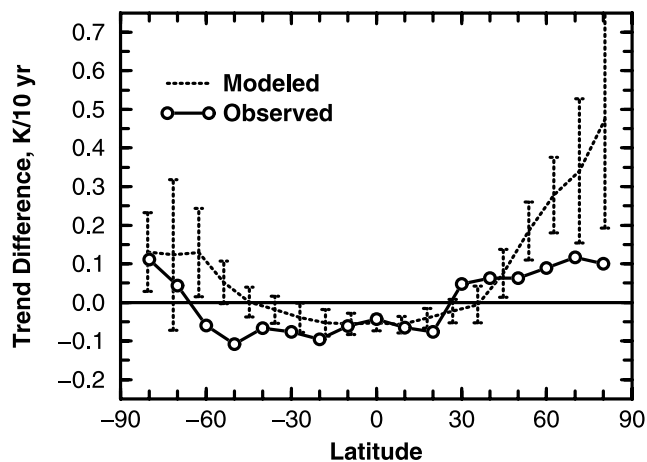


**Figure 10.** Differences between 1978–2004 trends in surface and troposphere air temperatures based on observations (Observed) and climate model (Modeled), i.e., difference of plots in Figures 8 and 9. These differences have different signs in low and high latitudes. Root mean errors of modeled differences (shown with vertical bars) were estimated from a 900-year control run of the same model.

[32] We do not see any serious inconsistencies between the 1978–2004 climatic trends observed by the MSU, surface temperature measurements, and climate model runs. The agreement between observations and the model give us more confidence in both. Furthermore, our results suggest a decreased vertical stability of the atmosphere (with the surface warming faster than the troposphere) in high and middle latitudes and an increasing stability (surface warming more slowly than the troposphere) at low latitudes, which we also find in model simulations of contemporary climate change. This result was predicted long ago by climate models [Manabe and Wetherald, 1975; Hansen *et al.*, 1984] and later found in observations from the global radiosonde network [Vinnikov *et al.*, 1996]. Although there is much uncertainty in the forcings used [Ramaswamy *et al.*, 2001], in the model's response [Cubasch *et al.*, 2001], and in sampling the observational signal, the fact that the model and observations agree so closely gives us more confidence in both the observational record and in the model projections of future climate change. Santer *et al.* [2005], using Intergovernmental Panel on Climate Change Fourth Assessment simulations of contemporary (20th century) climate variations by 19 of the most comprehensive modern climate models, have shown that the tropical tropospheric amplification phenomenon is model independent, and provided a very clear physical explanation.

## 7. Additional Uncertainty in Satellite Data

[33] Grody *et al.* [2004] pointed out that if we know that one instrument is much better calibrated than the others, this instrument could be chosen as an unbiased reference instrument, i.e.,  $\delta T = \delta U = 0$ . Since we have no such a priori knowledge, we assumed that one of the radiometers, NOAA-10, has a zero offset (i.e.,  $\delta T_{NOAA-10} = 0$ ), since this assumption does not affect the trend estimate. It is

possible, however, that one of the instruments is really much better calibrated than all of the others. In such a case it should be chosen as reference instrument with the assumption that  $\delta T = \delta U = 0$ . Using this approach, Table 3 shows the resulting climatic trend in the globally averaged MSU channel 2 brightness temperature under the assumption that the calibration of one radiometer is error free. Note that all of the trend estimates are within the range of 0.20 K/10 yr to 0.27 K/10 yr. It is quite reasonable to expect that the true trend is somewhere inside of this interval, which is surprisingly small. The current best estimate of the trend, based on assumption that none of instruments is perfectly calibrated, is 0.20 K/10 yr (see Table 2). It is interesting, however, that all of the adjustment coefficients,  $\delta U$ , given in Table 1 have the same negative sign. It looks as if all nine MSU instruments have channel 2 calibration nonlinearity biased in the same direction, with the TIROS-N MSU radiometer having the smallest magnitude of adjustment,  $\delta U$ . By choosing this instrument as reference we obtain a global trend estimate the same 0.20 K/10 yr. It also looks as if the difference between instruments does not significantly increase the uncertainty in the global climate trend estimates. Furthermore, none of the instruments being used as reference decreases the global trend estimate below 0.20 K/10 yr.

[34] For completeness, we compare this latest trend of 0.20 K/10 yr with the first trend analysis of MSU channel 2 and AMSU channel 5 by Vinnikov and Grody [2003], which only considered constant biases (i.e.,  $\delta U = 0$  in (1)) and precalibrated the MSU's using earlier prelaunch nonlinear coefficients [Mo, 1995]. As a result, the global trend was 0.26 K/10 yr for the 24-year period ending in 2002. To obtain accurate comparisons, the Vinnikov and Grody [2003] technique was applied to the updated 26 years of MSU measurements, which were precalibrated using the latest prelaunch nonlinear coefficients [Mo *et al.*, 2001] used in this paper. These updated MSU measurements resulted in a different set of constant bias adjustments as well as a slightly smaller global trend of 0.24 K/10 yr. This trend is only a little larger than the 0.20 K/10 yr obtained here using the more accurate intersatellite calibration method [Grody *et al.*, 2004]. However, in addition to providing a more accurate trend, this latest technique automatically corrects for systematic errors in the prelaunch

**Table 3.** Global Trend of MSU Channel 2 Brightness Temperature Estimates Using Different MSU Instruments as Reference<sup>a</sup>

Reference MSU	Overlaps	
	12	8
TIROS-N	0.20	0.20
NOAA-6	0.22	0.22
NOAA-7	0.22	0.21
NOAA-8	0.23	0.24
NOAA-9	0.27	0.24
NOAA-10	0.26	0.23
NOAA-11	0.26	0.23
NOAA-12	0.23	0.21
NOAA-14	0.24	0.21

<sup>a</sup>Unit is K/10 yr. The column pertaining to overlaps = 12 means that all overlapping observations were used to estimate the calibration adjustment coefficients [Grody *et al.*, 2004]. The results based on overlaps = 8 means that only the eight longest satellite overlaps were used in estimating the calibration adjustments [Vinnikov and Grody, 2003].

nonlinear calibration coefficients so that the results are insensitive to changes in the MSU precalibration. In conclusion, we find that the best estimate of the globally averaged trend of MSU channel 2 is 0.20 K/10 yr, with a standard deviation of 0.05 K/10 yr (see Table 2), which compares very well with the trend obtained from surface reports.

## 8. Concluding Remarks

[35] Over the past 5 years, studies by different groups have been performed to resolve the inconsistency between the MSU measurements and surface reports. This work began primarily as a consequence of the Wallace *et al.* [2000] National Research Council Panel report entitled “Reconciling Observations of Global Temperature Change.” At that time, only the trend analysis of MSU data by Christy *et al.* [2000] of the University of Alabama, Huntsville (UAH) was considered, which concluded that the global trend from the MSU tropospheric channel was negligibly small (0.05 K/10 yr), whereas the trend based on surface reports was about 0.17 K/10 yr. To help resolve this inconsistency, the panel recommended that independent studies be performed, by providing other groups with the raw and processed MSU measurements. Three years later, Mears *et al.* [2003] used the same method of intercalibrating the satellite observations as Christy *et al.* [2000], but obtained a global trend of 0.12 K/10 yr. Mears *et al.* concluded that the difference had to do with the manner in which the limited NOAA-9 MSU data were merged in the UAH analysis. However, as described in Section 1, common to both analyses was the empirical adjustment of the MSU’s based solely on the warm target temperature. The problem with their procedure is that the trend-like variation of the warm target temperature (due to orbital decay) is included in their adjusted measurements. Vinnikov and Grody [2003] recognized that the empirical adjustment developed by the UAH group modifies and can reduce the real climatic trend, so that it was not used in their analysis of MSU data. Consequently, they obtained a global trend between 0.22 and 0.26 K/10 yr. More recently, Grody *et al.* [2004] developed a more accurate technique of intercalibrating the MSU’s based on the physical characteristics of the instruments, which includes the uncertainties in the calibration targets and nonlinearity (equation (1)). The improved calibration adjustments have been applied in this paper and result in a globally averaged trend of 0.20 K/10 yr (Table 2). This trend is a little larger than the trend in surface records and than the latest trend estimate obtained from radiosonde records by Sherwood *et al.* [2005], who recognized that the inhomogeneity associated with radiosonde measurements [Lanzante *et al.*, 2003a, 2003b] can be significantly reduced by using only nighttime data. However, the trend in globally averaged tropospheric temperature has a minimum in the nighttime, so we would expect the actual trend to be larger than the estimate by Sherwood *et al.* [2005]. The trends in zonal averages of MSU channel 2 tropospheric temperature and in surface air temperature estimated in this paper should be considered as observational evidence of tropical tropospheric amplification phenomenon, previously known mostly from climate models [e.g., Vinnikov *et al.*, 1996].

[36] The recent publication by Fu *et al.* [2004] evaluates the stratospheric influence on the MSU channel 2 measurements. It also attempts to reduce the stratospheric contribution in the measurements by combining channel 2 with the stratospheric channel 4. Others have also discussed the relationship between the two channels [Tett and Thorne, 2004; Gillett *et al.*, 2004]. Unfortunately, uncertainties in calibration as well as the statistical nature of the different channel responses can result in large errors when combining these widely vertically separated channels to reduce the stratospheric contribution in channel 2. We can give an illustration of these effects by answering the question of why is there no signature of two major volcanic eruptions (El Chichón in 1982, and Pinatubo in 1991) in the time series of zonal temperature anomalies shown in Figure 7. It is well known that volcanic stratospheric aerosols cause surface (and tropospheric) cooling of a few tenths of a degree (K) and stratospheric warming of the order of a few degrees [Robock, 2000]. However, as mentioned in the introduction, the MSU channel 2 weighting function integrates these changes with weights of about 0.9 and 0.1 correspondingly and therefore averages out the two opposing temperature changes due to volcanic eruptions. This cancellation effect for MSU channel 2 is approximately correct for volcanic effects but obviously depends critically on the vertical structure of the temperature profile. It is also evident that any errors in calibration of these two channels can result in large errors when combining the channels to remove the stratospheric contribution in channel 2. As explained in section 1, it is for this reason that we compare the MSU channel 2 measurements directly with forward model calculations that include the stratospheric contribution, rather than attempt to correct the measurements for stratospheric effects.

[37] **Acknowledgments.** K. Y. V. acknowledges support by NOAA through NESDIS and OGP grants to CICS. P. D. J. was supported by the Office of Science (BER), U.S. Dept. of Energy, grant DE-FG02-98ER62601. A. R. was supported by National Science Foundation grant ATM-0313592. The views expressed in this publication are those of the authors and do not necessarily represent those of NOAA. We thank J. Lanzante, T. Knutson, B. Soden, A. Leetmaa, J. Sullivan, D. Tarpley, A. Powell, and two anonymous reviewers for their useful comments and discussions, and Z. Chang for initial processing of the satellite data.

## References

- Christy, J. R., and W. B. Norris (2004), What may we conclude about global tropospheric temperature trends?, *Geophys. Res. Lett.*, *31*, L06211, doi:10.1029/2003GL019361.
- Christy, J. R., R. W. Spencer, and W. D. Braswell (2000), MSU tropospheric temperatures: Dataset construction and radiosonde comparisons, *J. Clim.*, *17*, 1153–1170.
- Cubasch, U., *et al.* (2001), Projections of future climate change, in *IPCC, Climate Change 2001—The Scientific Basis*, edited J. T. Houghton, pp. 525–582, Cambridge Univ. Press, New York.
- Dai, A., and K. E. Trenberth (2004), The diurnal cycle and its depiction in the Community Climate System Model, *J. Clim.*, *17*, 930–951.
- Delworth, T. L., and T. R. Knutson (2000), Simulation of early 20th century global warming, *Science*, *287*, 2246–2250.
- Delworth, T. L., *et al.* (2002), Review of simulations of climate variability and change with the GFDL R30 coupled climate model, *Clim. Dyn.*, *19*, 555–574.
- Fu, Q., and C. M. Johanson (2005), Satellite-derived vertical dependence of tropical tropospheric temperature trends, *Geophys. Res. Lett.*, *32*, L10703, doi:10.1029/2004GL022266.
- Fu, Q., C. M. Johanson, S. G. Warren, and D. J. Seidel (2004), Contribution of stratospheric cooling to satellite-inferred tropospheric temperature trends, *Nature*, *429*, 55–58.

- Gillett, N. P., B. D. Santer, and A. J. Weaver (2004), Stratospheric cooling and the troposphere, *Nature*, *432*, doi:10.1038/nature03209.
- Grody, N. C., K. Y. Vinnikov, M. D. Goldberg, J. T. Sullivan, and J. D. Tarpley (2004), Calibration of multi-satellite observations for climatic studies: Microwave Sounding Unit (MSU), *J. Geophys. Res.*, *109*, D24104, doi:10.1029/2004JD005079.
- Hansen, J., et al. (1984), Climate sensitivity: Analysis of feedback mechanisms, in *Climate Processes and Climate Sensitivity*, *Geophys. Monogr. Ser.*, vol. 29, edited by J. E. Hansen and T. Takahashi, pp. 130–163, AGU, Washington, D. C.
- Ignatov, A., I. Laszlo, E. D. Harrod, K. B. Kidwell, and G. P. Goodrum (2004), Equator crossing times for NOAA, ERS and EOS sun-synchronous satellites, *Int. J. Remote Sens.*, *25*, 5255–5266.
- Jenkins, G. M., and D. G. Watts (1968), *Spectral Analysis and its Applications*, pp. 132–135, Holden Day, Boca Raton, Fla.
- Jones, P. D., and A. Moberg (2003), Hemispheric and large-scale surface air temperature variations: An extensive revision and an update to 2001, *J. Clim.*, *16*, 206–223.
- Lanzante, J. R., S. A. Klein, and D. J. Seidel (2003a), Temporal homogenization of monthly radiosonde temperature data: Part I. Methodology, *J. Clim.*, *16*, 224–240.
- Lanzante, J. R., S. A. Klein, and D. J. Seidel (2003b), Temporal homogenization of monthly radiosonde temperature data: Part II. Trends, sensitivities, and MSU comparison, *J. Clim.*, *16*, 241–262.
- Manabe, S., and R. Wetherald (1975), The effect of doubling the CO<sub>2</sub> concentration on the climate of a general circulation model, *J. Atmos. Sci.*, *32*, 3–15.
- Manabe, S., R. J. Stouffer, M. J. Spelman, and K. Bryan (1991), Transient response of a global ocean-atmosphere model to gradual changes of atmospheric CO<sub>2</sub>: Part I. Annual mean response, *J. Clim.*, *4*, 785–818.
- Mears, C. A., M. C. Schabel, and F. J. Wentz (2003), A reanalysis of the MSU channel 2 tropospheric temperature record, *J. Clim.*, *16*, 3650–3664.
- Mo, T. (1995), A study of the Microwave Sounding Unit on the NOAA-12 satellite, *IEEE Trans. Geosci. Remote Sens.*, *33*, 1141–1152.
- Mo, T., M. D. Goldberg, and D. S. Crosby (2001), Recalibration of the NOAA Microwave Sounding Unit, *J. Geophys. Res.*, *106*, 10,145–10,150.
- Ramaswamy, V., et al. (2001), Radiative forcing of climate change, in *IPCC, Climate Change 2001—The Scientific Basis*, edited by J. T. Houghton et al., pp. 350–414, Cambridge Univ. Press, New York.
- Rayner, N. A., et al. (2003), Global analyses of sea surface temperature, sea ice, and night marine air temperature since the late nineteenth century, *J. Geophys. Res.*, *108*(D14), 4407, doi:10.1029/2002JD002670.
- Robock, A. (2000), Volcanic eruptions and climate, *Rev. Geophys.*, *38*, 191–219.
- Santer, B. D., et al. (2005), Amplification of surface temperature trends and variability in the tropical atmosphere, *Science*, *309*, 1551–1556.
- Sherwood, S. C., J. R. Lanzante, and C. L. Meyer (2005), Radiosonde daytime biases and late-20th century warming, *Science*, *309*, 1556–1559.
- Swanson, R. E. (2003), Evidence of possible sea-ice influence on Microwave Sounding Unit tropospheric temperature trends in polar regions, *Geophys. Res. Lett.*, *30*(20), 2040, doi:10.1029/2003GL017938.
- Tett, S., and P. Thorne (2004), Tropospheric temperature series from satellites, *Nature*, *432*, doi:10.1038/nature03208.
- Thompson, D. W. J., and S. Solomon (2002), Interpretation of Southern Hemisphere climate change, *Science*, *296*, 895–899.
- Vinnikov, K. Y. (1986), *Climate Sensitivity* (in Russian), 224 pp., Gidrometeoizdat, St. Petersburg.
- Vinnikov, K. Y., and N. C. Grody (2003), Global warming trend of mean tropospheric temperature observed by satellites, *Science*, *302*, 269–272.
- Vinnikov, K. Y., A. Robock, R. J. Stouffer, and S. Manabe (1996), Vertical patterns of free and forced climate variations, *Geophys. Res. Lett.*, *23*, 1801–1804.
- Vinnikov, K. Y., A. Robock, N. C. Grody, and A. Basist (2004), Analysis of diurnal and seasonal cycles and trends in climatic records with arbitrary observation times, *Geophys. Res. Lett.*, *31*, L06205, doi:10.1029/2003GL019196.
- Wald, A. (1940), The fitting of straight lines if both variables are subject to error, *Ann. Math. Stat.*, *11*, 284–300.
- Wallace, J. M., et al. (2000), *Reconciling Observations of Global Temperature Change*, 85 pp., Natl. Acad. Sci., Washington, D. C.

---

M. D. Goldberg and N. C. Grody, Center for Satellite Applications and Research, NOAA/NESDIS, 5200 Auth Road, Camp Springs, MD 20746, USA. (mitch.goldberg@noaa.gov; ngantique@hotmail.com)

P. D. Jones, Climate Research Unit, University of East Anglia, Norwich, NR4 7TJ, UK. (p.jones@uea.ac.uk)

A. Robock, Department of Environmental Sciences, Rutgers University, 14 College Farm Road, New Brunswick, NJ 08901-8551, USA. (roboc@envsci.rutgers.edu)

R. J. Stouffer, Geophysical Fluid Dynamics Laboratory, NOAA, Princeton University Forrestal Campus, 201 Forrestal Road, Princeton, NJ 08540-6649, USA. (ronald.stouffer@noaa.gov)

K. Y. Vinnikov, Department of Atmospheric and Oceanic Science, University of Maryland, College Park, MD 20742, USA. (kostya@atmos.umd.edu)